Electronic Supplementary Information

Highly Conductive and Stable Hybrid Solid Electrolyte for High Voltage Lithium Metal Batteries

Jiangtao Yu, [1, †] Yin Hu, [1,†] Xinyu Ma,[1] Xiuyang Zou,[1] Haojun Qi,[1] Yingjie Zhou[2] and Feng Yan [1,*]

[1]Jiangsu Engineering Laboratory of Novel Functional Polymeric Materials College of Chemistry, Chemical Engineering and Materials Science Soochow University, Suzhou 215123, China

[2]State Key Laboratory for Modification of Chemical Fibers and Polymer Materials, College of Materials Science and Engineering Donghua University, Shanghai 201620, China

* Correspondence to fyan@suda.edu.cn (F. Y.)

†Authors with equal contributions.

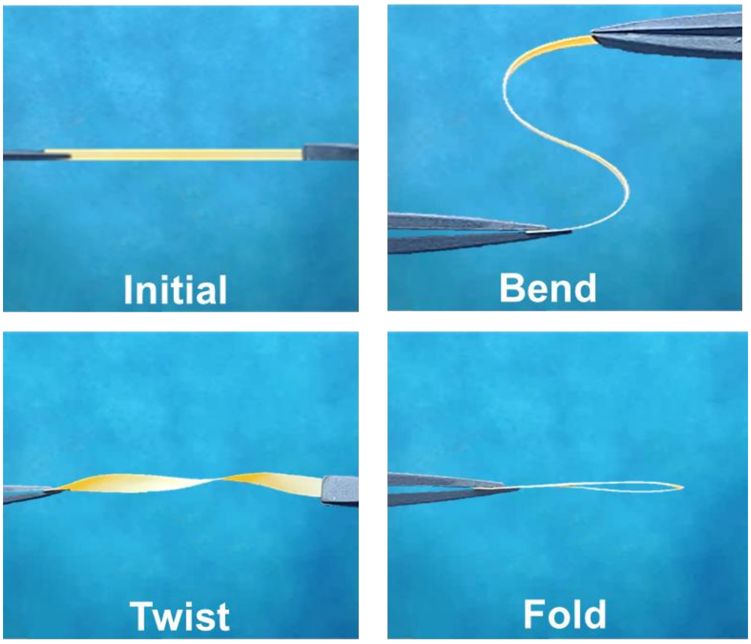

Figure S1. Images of P(VDF-HFP)-Li10-50LATP HSE with bending, twisting and folding. The prepared HSE has good mechanical strength and flexibility.

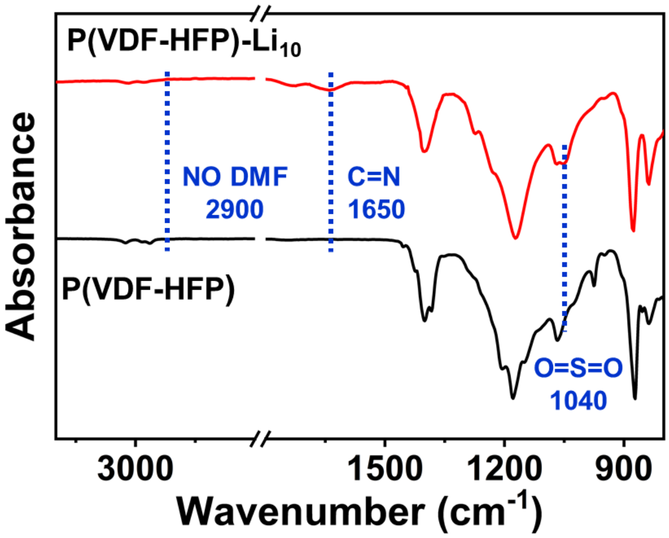

Figure S2. FTIR spectra of P(VDF-HFP), P(VDF-HFP)-Li10 polymer (without LiTFSI). The C=N and O=S=O peaks belonging to the grafted polymer appear at 1650 cm^{-1} and 1040 cm^{-1}. The electrolyte does not contain residues of the solvent DMF.

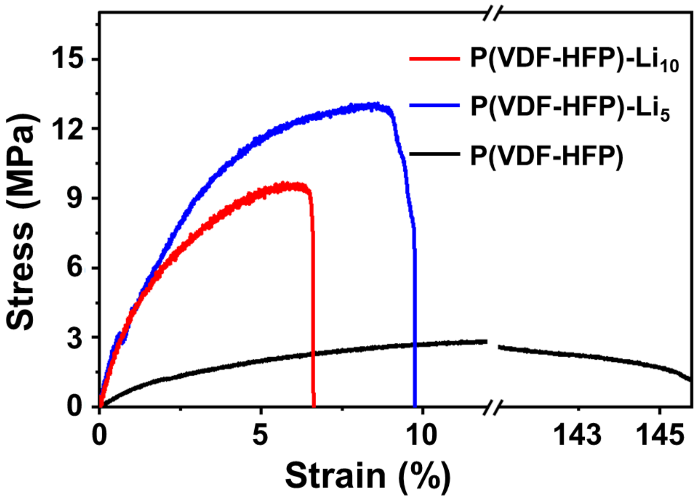

Figure S3. Tensile strain test of P(VDF-HFP) membrane with different grafting amounts of lithium taurine. As the charge density in the polymer increases, the polymer chain becomes more standardized, which increases the tensile stress and decreases the tensile strain of the polymer after grafting.

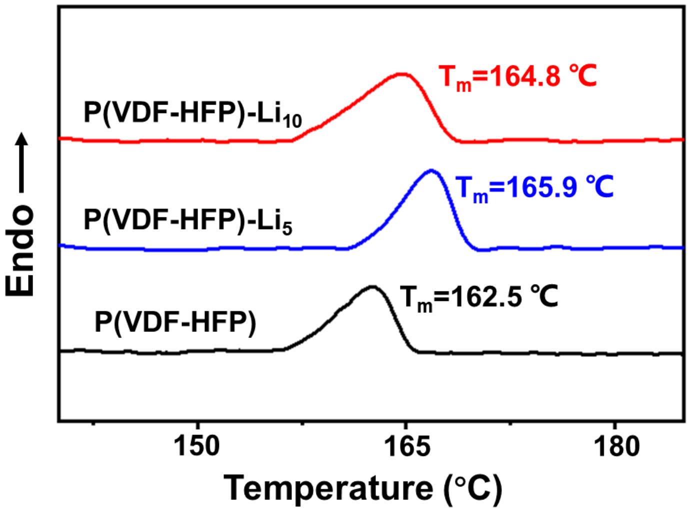

Figure S4. DSC heating curves of different amounts of lithium taurine to P(VDF-HFP) at 10 °C min^{-1} under flowing N_2. Under the influence of the side chain groups, the melting peak (T_m) of P(VDF-HFP)-Li_5 increases, while T_m of the P(VDF-HFP)-Li_{10} decreases because of the increased charge density.

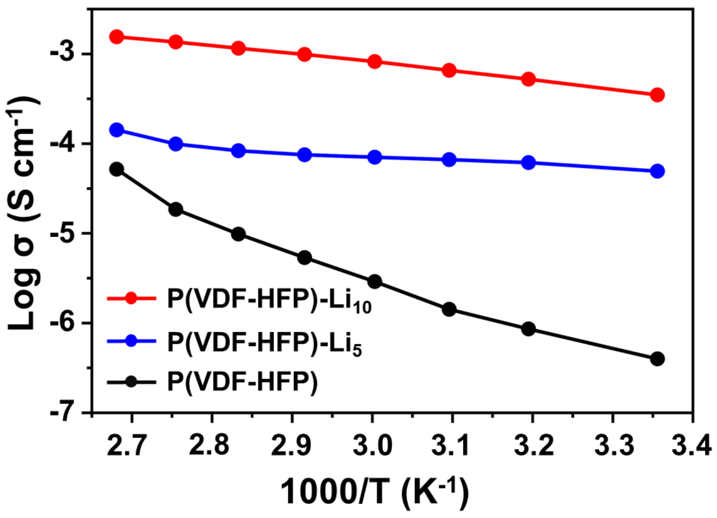

Figure S5. Temperature dependence of the Li^+ conductivity for P(VDF-HFP), P(VDF-HFP)-Li_5, P(VDF-HFP)-Li_{10} polymer electrolyte from 25 °C to 100 °C, and the activation energy of ion migration was calculated by the Arrhenius formula. Compared with P(VDF-HFP), the grafted polymer has high ionic conductivity and low activation energy.

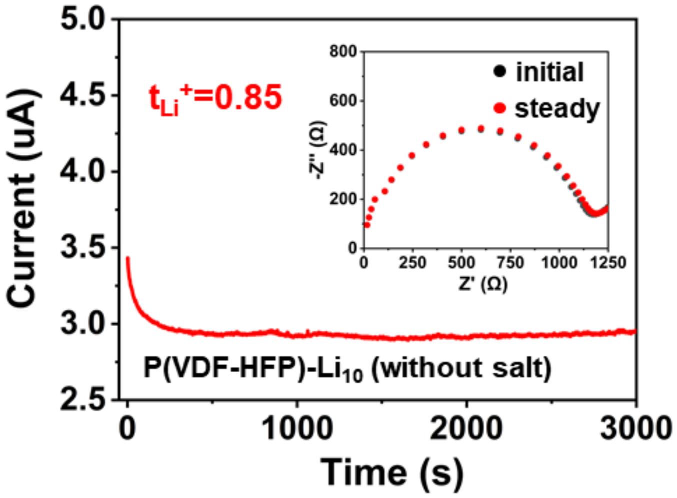

Figure S6. Current-time curves following DC polarization of grafted polymer P(VDF-HFP)-Li_{10} without LiTSFI. The t_{Li}^+ of P(VDF-HFP)-Li_{10} polymer is 0.85, which indicates the grafted polymer P(VDF-HFP)-Li_{10} has a strong Li^+ transport ability.

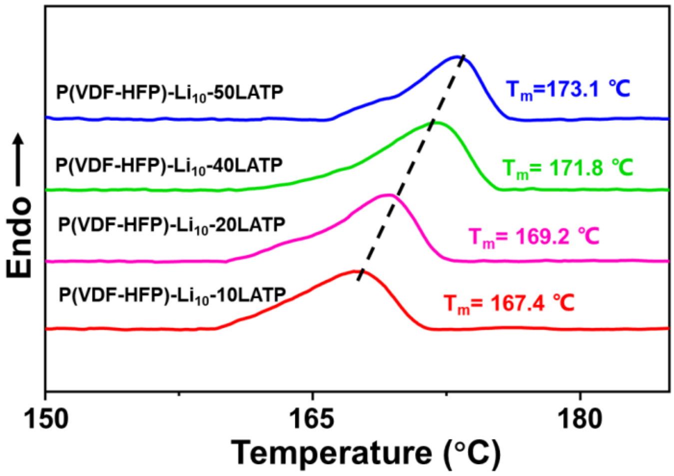

Figure S7. DSC heating curves of the HSE with different LATP content at 10 °C min^{-1} under flowing N_2. The melting point (T_m) of the HSE increases as the content of LATP particles increases.

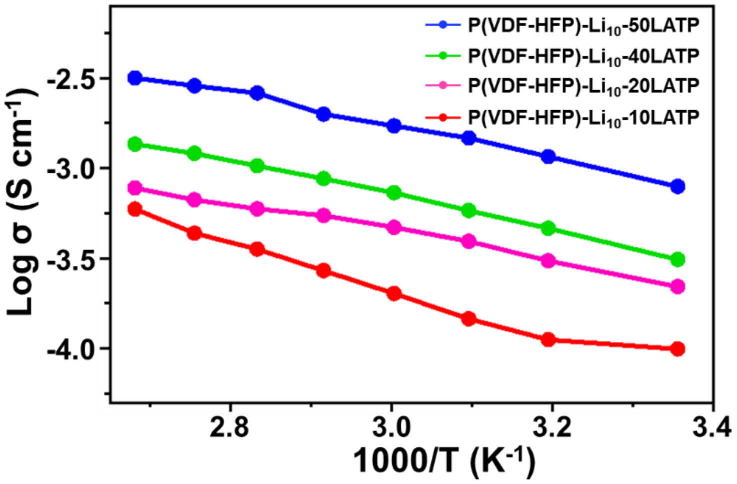

Figure S8. Temperature-dependent with Li$^+$ conductivity for the HSE with different LATP contents from 25 °C to 100 °C. As the contents of LATP enhances, the ionic conductivity of HSE increases.

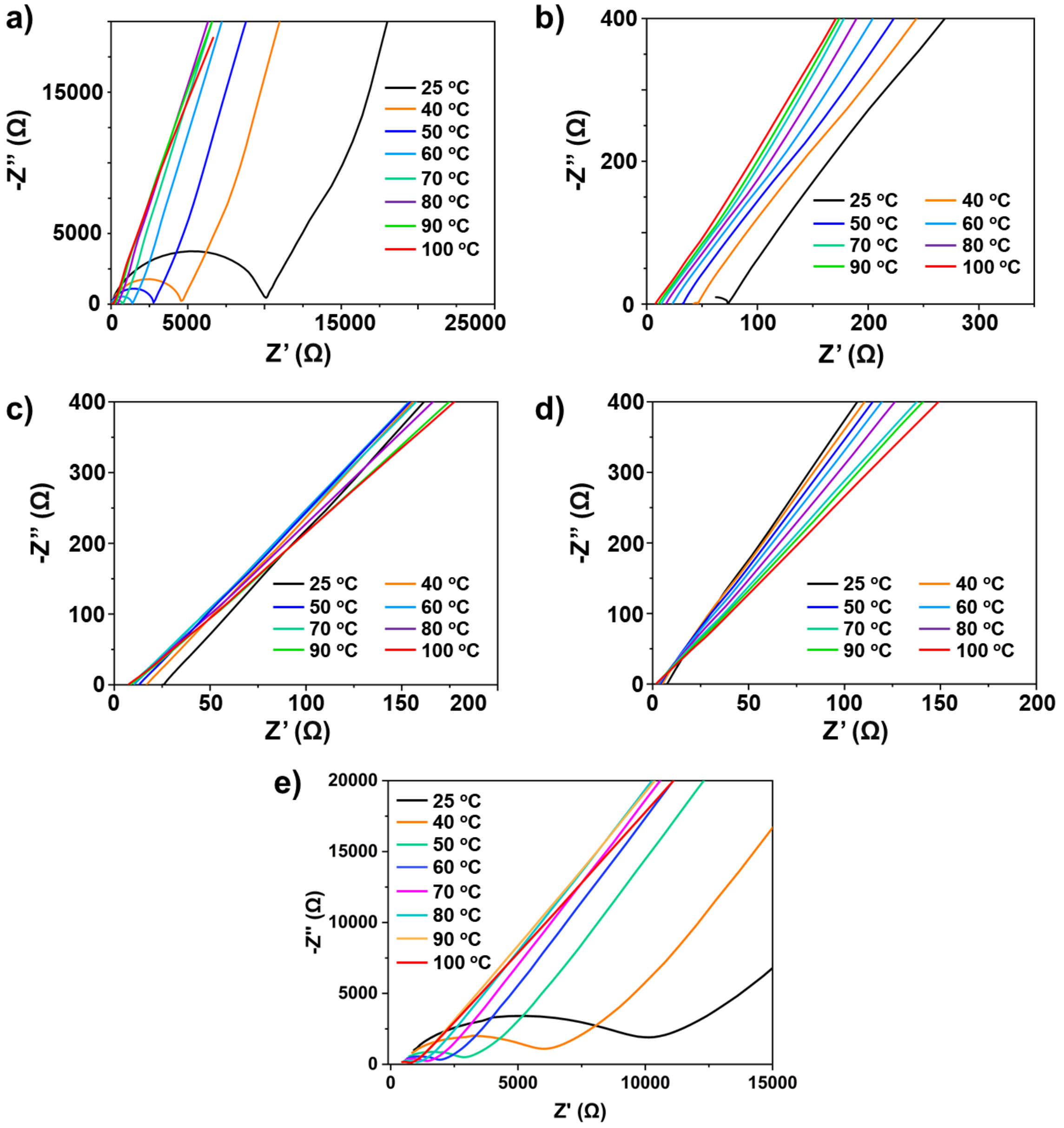

Figure S9. AC impedance spectra of a) P(VDF-HFP), b) P(VDF-HFP)-Li$_{10}$, c) P(VDF-HFP)-50LATP, d) P(VDF-HFP)-Li$_{10}$-50LATP and e) LATP ceramic electrolyte at different temperatures.

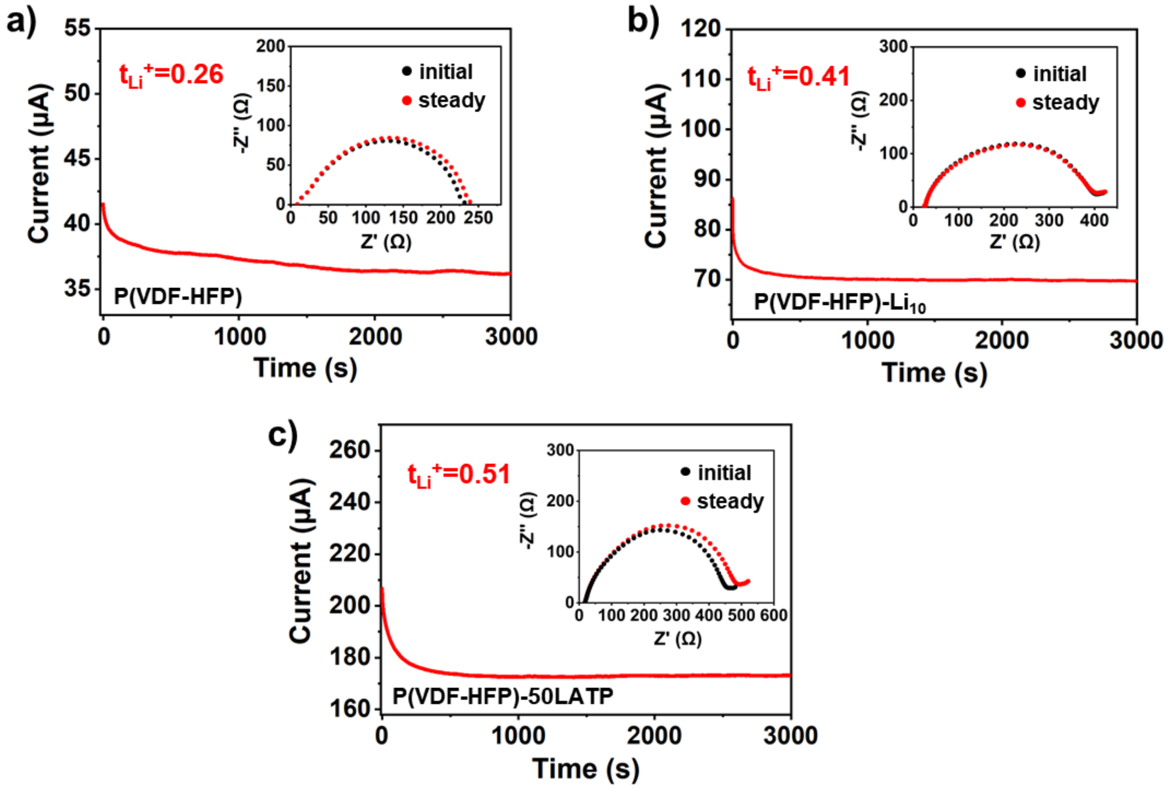

Figure S10. Current-time curves following DC polarization of a) P(VDF-HFP), b) P(VDF-HFP)-Li$_{10}$, c) P(VDF-HFP)-50LATP under an applied voltage of 10 mV. The insets are AC impedance spectra of each electrolyte, respectively.

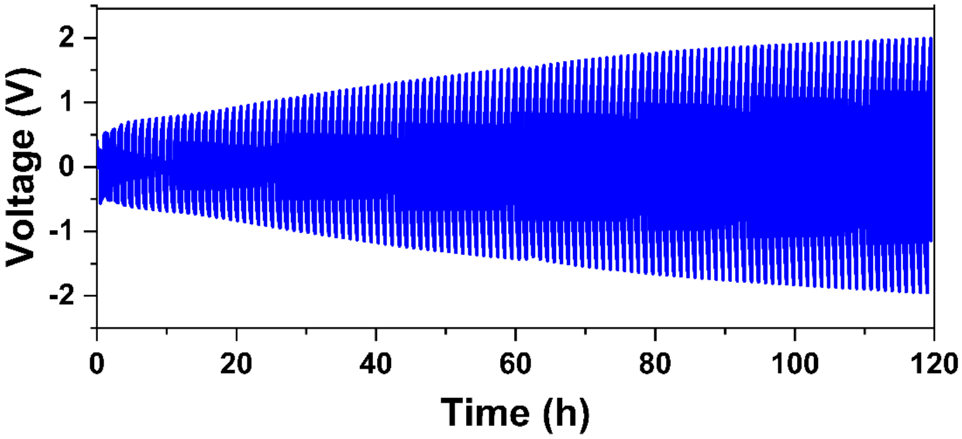

Figure S11. Voltage profile of the lithium symmetric cells cycling curves with LATP electrolyte at the current density of 0.1 mA cm^{-2}.

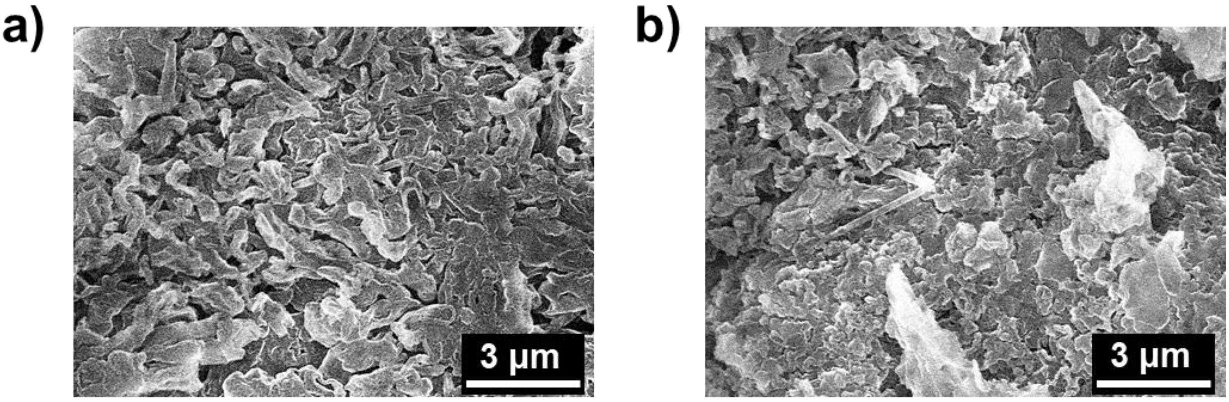

Figure S12. SEM images of Li surface of a) P(VDF-HFP)-Li$_{10}$ after 650 h symmetric cell cycling at 0.1 mA cm^{-2} and b) Li electrode with LATP ceramics after 60 h symmetric cell cycling at 0.1 mA cm^{-2}. The LATP electrolytes lead to uneven lithium deposition with lithium dendrites.

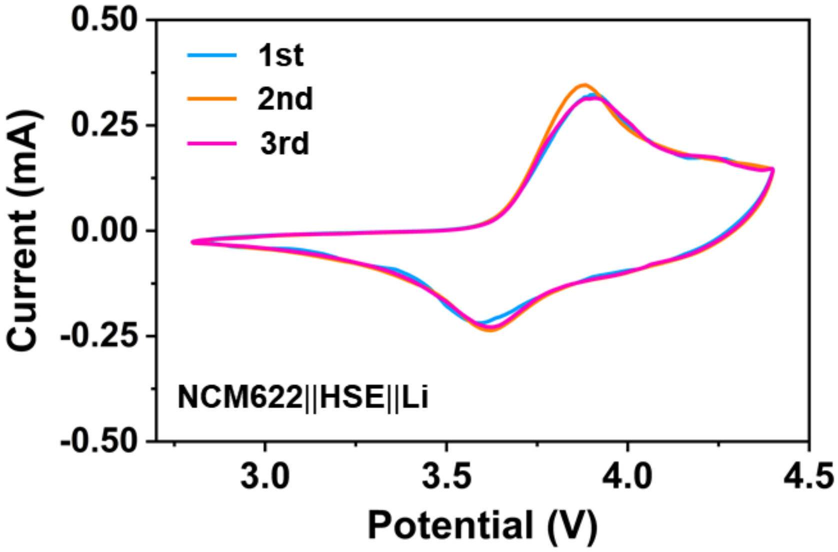

Figure S13. Cyclic voltammetry (CV) curve of NCM622||HSE||Li cell between 2.8 V-4.3 V at 0.1 mV s^{-1}.

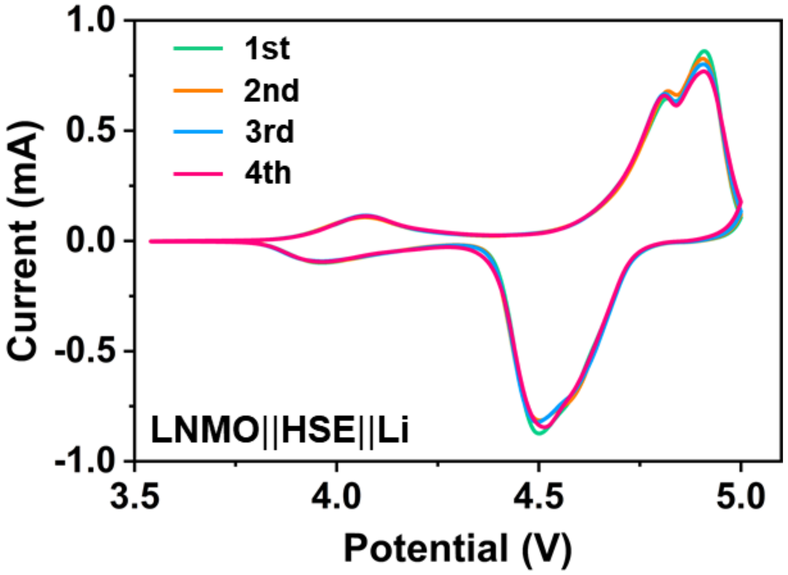

Figure S14. Cyclic voltammetry (CV) curve of LNMO||HSE||Li cell between 3.5 V-5 V at 0.1 mV s^{-1}.

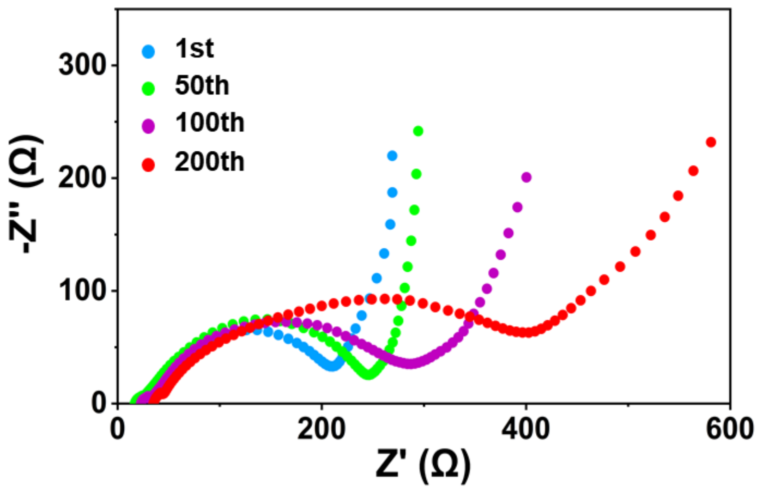

Figure S15. Nyquist plots of LNMO||Li solid-state battery after different cycles.

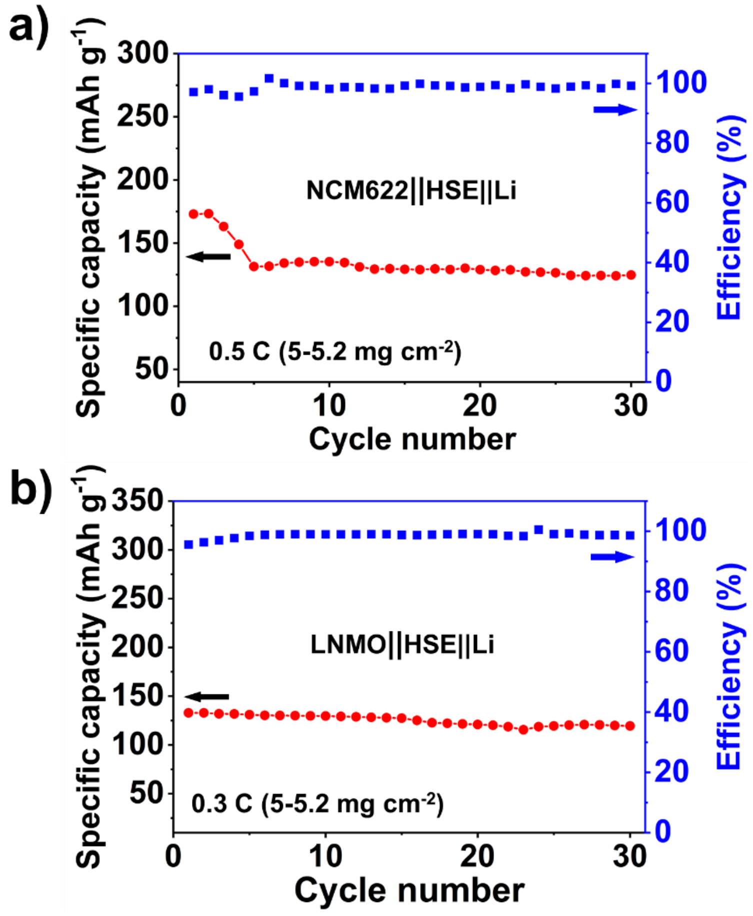

Figure S16. Cycling performance of a) NCM622||Li at 0.5 C and b) LNMO||Li at 0.3 C cells with high cathode loading (5-5.2 mg cm^{-2}).

Table S1. Elemental content analysis results for P(VDF-HFP)-Li_{10}.

Element	**F**	**C**	**O**	**S**	**N**
At %	**49.2**	**39.9**	**9.9**	**0.7**	**0.3**

Table S2. Ionic conductivity and activation energy at 25 °C of P(VDF-HFP), P(VDF-HFP)-Li_5 and P(VDF-HFP)-Li_{10} electrolyte.

	P(VDF-HFP)	**P(VDF-HFP)-Li_5**	**P(VDF-HFP)-Li_{10}**
R_b (Ω)	10090	78.04	47.45
Thickness (μm)	71	68	94
Ion conductivity (S cm^{-1})	3.52×10^{-7}	4.36×10^{-5}	9.91×10^{-5}
Activation energy (eV)	0.61	0.12	0.24

Table S3. Ionic conductivity and activation energy at 25 °C of P(VDF-HFP)-Li_{10} with different LATP contents.

	P(VDF-HFP)-Li_{10} -10LATP	**P(VDF-HFP)-Li_{10} -20LATP**	**P(VDF-HFP)-Li_{10} -40LATP**	**P(VDF-HFP)-Li_{10} -50LATP**
R_b (Ω)	14.33	25.01	17.66	7.54
Thickness (μm)	94	125	154	119
Ion conductivity (S cm^{-1})	2.20×10^{-4}	2.51×10^{-4}	4.38×10^{-4}	7.88×10^{-4}
Activation energy (eV)	0.16	0.15	0.22	0.18

Table S4. Recent literatures on the electrochemical performance of hybrid solid-state electrolytes.

Inorganic	Polymer	σ (mS cm^{-1})	t_{Li^+}	Potential (V vs. Li/Li$^+$)	Ref.
LLZO	**PEO/LiTFSI**	**0.25**	**--**	**4**	**a** [S1]
	P(VDF-HFP)	**0.11**	**--**	**4.5**	**c** [S2]
LATP	**PEO/LiTFSI/PAN**	**0.05**	**0.32**	**4.8**	**j** [S3]
	PVDF/LiClO$_4$	**0.12**	**0.54**	**4.5**	**d** [S4]
LAGP	**PEO/LiTFSI**	**0.52**	**--**	**4.3**	**f** [S5]
LAHP	**PEO/LiTFSI**	**0.08**	**0.35**	**4.5**	**b** [S6]
Al-LLZTO	**P(VDF-HFP)/LiTFSI**	**0.18**	**0.69**	**4.7**	**i** [S7]
LLZTO	**P(VDF-HFP)/LiTFSI/LiBOB**	**0.074**	**--**	**5.0**	**e** [S8]
	PAN/LiTFSI	**0.6**	**0.42**	**4.8**	**k** [S9]
Lepidolite	**PVDF/LiClO$_4$**	**0.61**	**--**	**4.7**	**l** [S10]
SiO$_2$	**PEO/LiTFSI**	**0.6**	**--**	**4.5**	**g** [S11]
	PEO/ILs/LiTFSI	**0.34**	**0.14**	**4.4**	**m**[S12]
LLZTO	**PVDF/PVAC-LiClO$_4$**	**0.48**	**0.43**	**4.6**	**h** [S13]
LATP	**Grafted P(VDF-HFP)/LiTFSI**	**0.79**	**0.61**	**5.16**	**This work**

Video S1. COMSOL Multiphysics Simulation of Different HSEs Current Density.

Video S2. Soft-packed Lithium-ion Battery Safety Test.

References

S1 L. Chen, Y. Li, S. P. Li, L. Z. Fan, C. W. Nan and J. B. Goodenough, *Nano Energy*, 2018, **46**, 176–184.

S2 W. Zhang, J. Nie, F. Li, Z. L. Wang and C. Sun, *Nano Energy*, 2018, **45**, 413–419.

S3 Y. Zhao, Y. Bai, Y. Bai, M. An, G. Chen, W. Li, C. Li and Y. Zhou, *J. Power Sources*, 2018, **407**, 23–30.

S4 D. Li, L. Chen, T. Wang and L. Z. Fan, *ACS Appl. Mater. Interfaces*, 2018, **10**, 7069–7078.

S5 P. Yao, B. Zhu, H. Zhai, X. Liao, Y. Zhu, W. Xu, Q. Cheng, C. Jayyosi, Z. Li, J. Zhu, K. M. Myers, X. Chen and Y. Yang, *Nano Lett.*, 2018, **18**, 6113–6120.

S6 H. Zhai, P. Xu, M. Ning, Q. Cheng, J. Mandal and Y. Yang, *Nano Lett.*, 2017, **17**, 3182–3187.

S7 X. Wang, Y. Zhang, X. Zhang, T. Liu, Y. H. Lin, L. Li, Y. Shen and C. W. Nan, *ACS Appl. Mater. Interfaces*, 2018, **10**, 24791–24798.

S8 Z. Yao, Y. Kang, M. Hou, J. Huang, J. Zhang, B. Yang, Y. Dai and F. Liang, *Adv. Funct. Mater.*, 2022, **2111919**, 1–10.

S9 H. Zhang, C. Li, M. Piszcz, E. Coya, T. Rojo, L. M. Rodriguez-Martinez, M. Armand and Z. Zhou, *Chem. Soc. Rev.*, 2017, **46**, 797–815.

S10 S. Hao, L. Li, W. Cheng, Q. Ran, Y. Ji, Y. Wu, J. Huo, Y. Yang and X. Liu, *J. Mater. Chem. A*, 2022, **10**, 4881-4888.

S11 B. Wang, Y. Wu, S. Zhuo, S. Zhu, Y. Chen, C. Jiang and C. Wang, *J. Mater. Chem. A*, 2020, **8**, 5968–5974.

S12 G. Yang, Y. Song and L. Deng, *J. Mater. Chem. A*, 2021, **9**, 6881–6889.

S13 L. Li, H. Duan, J. Li, L. Zhang, Y. Deng and G. Chen, *Adv. Energy Mater.*, 2021, **11**, 1–32.